Spectroscopy and Photochemistry; General Theory

Light-Harvesting with Guide-Slide Superabsorbing Condensed-Matter Nanostructures

William Myles Brown, and Erik Manuel Gauger

Just Accepted

Light-Harvesting with Guide-Slide Superabsorbing Condensed-Matter Nanostructures

W.M. Brown* and E.M. Gauger*

SUPA, Institute of Photonics and Quantum Sciences, Heriot-Watt University, EH14 4AS Edinburgh, United Kingdom

E-mail: wmb1@hw.ac.uk; e.gauger@hw.ac.uk

Abstract

We establish design principles for light-harvesting antennae whose energy capture scales superlinearly with system size. Controlling the absorber dipole orientations produces sets of 'guide-slide' states which promote steady-state superabsorbing characteristics in noisy condensed-matter nanostructures. Inspired by natural photosynthetic complexes, we discuss the example of ring-like dipole arrangements and show that, in our setup, vibrational relaxation enhances rather than impedes performance. Remarkably, the superabsorption effect proves robust to $\mathcal{O}(5\%)$ disorder simultaneously for all relevant system parameters, showing promise for experimental exploration across a broad range of platforms.

Graphical TOC Entry
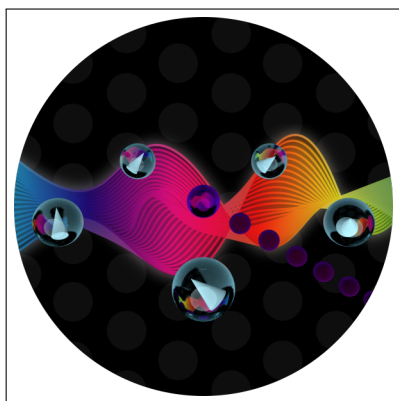
Introduction – Photosynthesis powers most life on Earth[1] and may provide templates for artificial light-harvesting.[2–4] Recent years have seen several proposals for enhancing the performance of quantum photocells beyond the venerable Shockley-Queisser limit of traditional photovoltaic devices.[5] Many of these aim to prevent recombination once a photon has been absorbed, e.g. through interference in multi-level systems[6,7] or as dark-state protection with multiple interacting dipoles.[8–11] Optical ratcheting[12,13] may offer further advantages by allowing an antenna to keep absorbing whilst being immune to recombination. Recent work underlines the importance of expanding beyond the single excitation subspace even in the presence of exciton-exciton annihilation.[12,14] Further, it has also been proposed that coherent vibrations,[15,16] as well as excitonic coherences[17] could be beneficial.

An alternative approach to improving the performance of light harvesters would be to enhance the effective optical absorption rate. In 1954 Dicke predicted the phenomenon of superradiance, where N atoms exhibit a collectively-enhanced 'greater-than-the-sum-of-its-parts' emission rate $\propto N^2$.[18] The possibility of harnessing the time-reversed phenomena has recently been proposed: (slightly) lifting degeneracies through symmetric dipolar interactions allows environmental control which temporarily keeps the system in a regime where it dis-

plays 'superabsorption'.[19] This does not occur in natural systems but was inspired by photo-synthetic ring antenna surrounding a reaction centre that converts optically-created excitations into useful chemical energy.[20,21] In natural rings, dipoles tend to align tangentially around the ring,[22] limiting the overall light-matter coupling but also allowing for inclusion of mechanisms for safeguarding against photo-damage.[23] On the other hand, for artificial systems configurations with a stronger collective dipole may prove more advantageous, as we explore in the following.

A very recent experimental study reports the observation of superabsorption with atomic systems,[24] providing a strong motivation for tackling the challenge of harnessing collectively enhanced absorption in condensed matter and particularly molecular structures. Encouragingly, molecular rings displaying coherence effects can be synthesised,[25,26] and cooperative dipole behaviour remains attainable under strong dephasing.[27] Delocalised excitonic states of the kind necessary for the proposals listed above may also occur in stacks of rings which self assemble into symmetric nanotubes.[28,29]

In this Letter, we examine the potential of condensed-matter nanostructures to operate as collectively-enhanced quantum photocells. Finding that the geometry of Ref.[19] fails in the presence of vibrational relaxation, we focus on a different means of achieving a cooperative advantage. We define a *guide-slide superabsorber* to be a collection of optical dipoles possessing the following properties:

I. A ladder of excitation manifolds, each with rapid relaxation to a well-defined lowest energy state.

II. Collectively-enhanced optical rates linking the lowest energy states of adjacent manifolds.

III. Spectral selectivity allowing suppression of optical decay below an enhanced target transition.

We argue that ring-like arrangements of dipoles meet conditions I-III, provided the
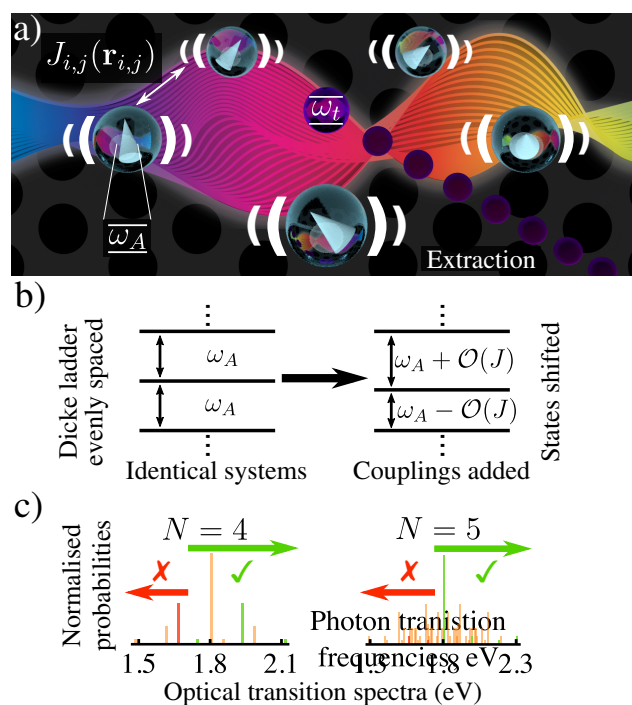
Figure 1: a) Artistic depiction of a guide-slide superabsorber: A ring of skewed optical dipoles interacting with a shared photon environment, local phonon baths, and a central extracting trap. A photonic crystal suppresses interaction with certain optical modes. b) Couplings $J_{i,j}$ between dipoles cause a perturbation to the Dicke ladder, primarily lifting the degeneracy of ladder rung spacings. c) Histogram of transition frequencies for coupled dipoles: there is no overlap between undesirable modes to be suppressed (red) and light-harvesting target modes (green) irrespective of ring size.[30]

alignment of dipoles is suitably skewed. While this skewness decreases the achievable degree of collective enhancement, crucially this configuration proves robust against the inclusion of phonons and significant levels of disorder: we demonstrate superlinear scaling of both optical absorption and net power output.

Model – We consider a ring of N optical dipoles (see Fig. 1a), each modelled as a degenerate two-level system (2LS) with transition energy $\omega_A = 1.8$ eV ($\hbar = 1$), near the peak of the solar power spectrum. Letting N uncoupled dipoles interact collectively with the electromagnetic environment leads to a Dicke ladder with $N+1$ equally spaced 'rungs' separated by steps of ω_A. Each rung represents a collective state for a different number of shared excitations, and optical rates near the middle of this ladder are collectively-enhanced and proportional to N^2.[18,31]

Interactions between dipoles perturb this picture, however, for moderate coupling strength, the system retains a ladder of eigenstates connected by enhanced optical transitions (Fig. 1b). The rungs are no longer evenly spaced, instead we obtain a chirped profile with a frequency increment determined by the strength of the dipolar couplings.[19] This is accompanied by a partial re-distribution of the oscillator strength away from ladder transitions, and a richer optical spectrum (Fig. 1c).

For closely spaced absorbers, dipolar interactions arise naturally from the 'cross Lamb-shift' (resonant Förster) terms in the many-body quantum optical master equation,[32–34]

$$J_{i,j}(\mathbf{r}_{i,j}) = \frac{1}{4\pi\epsilon_0 |\mathbf{r}_{i,j}|^3}\left(\mathbf{d}_i \cdot \mathbf{d}_j - \frac{3(\mathbf{r}_{i,j} \cdot \mathbf{d}_i)(\mathbf{r}_{i,j} \cdot \mathbf{d}_j)}{|\mathbf{r}_{i,j}|^2}\right)$$

where $\mathbf{r}_{i,j}$ is the vector linking the two dipoles i, j, and $\mathbf{d}_i$ is the dipole moment at site i whose strength is related to the natural lifetime τ_L of an isolated 2LS by $|\mathbf{d}| = \sqrt{3\pi\epsilon_0 \tau_L^{-1} c^3/\omega_A^3}$.[35,36]

Employing the usual definition of site-defined Pauli operators, the ring Hamiltonian reads

$$\hat{H}_{\mathrm{ring}} = \omega_A \sum_{i=1}^{N} \hat{\sigma}_i^z + \sum_{i,j=1}^{N} J_{i,j}(\mathbf{r}_{i,j})(\hat{\sigma}_i^+ \hat{\sigma}_j^- + \hat{\sigma}_i^- \hat{\sigma}_j^+) .$$

$$(1)$$

Assuming a ring diameter that is small compared to relevant photon wavelengths ($\sim 2\pi c/\omega_A$) we may neglect phase factors in the coupling elements and write the optical interaction Hamiltonian as

$$\hat{H}_{I,\mathrm{opt}} = \sum_{i=1}^{N} \mathbf{d}_i \hat{\sigma}_i^x \otimes \sum_k f_k(\hat{a}_k + \hat{a}_k^\dagger) ,\qquad (2)$$

where f_k and $\hat{a}_k^{(\dagger)}$ are, respectively, the coupling strength and annihilation (creation) operator for the optical mode k.[19,34]

We begin by contrasting a ring of dipoles that are all perpendicular to the plane of the ring (||-SA) to the guide-slide setup (GS-SA), where each dipole has been tilted 'sideways' by $\theta_{\mathrm{zen}} = \pi/4$ (see Fig. 1a and Supplementary Information (SI)[30]). The purpose of this tilting is to flip the sign of nearest-neighbour $J_{i,j}$ terms in Eq. (1) whilst preserving a substantial collective dipole strength $\mathbf{D} = \sum_i^N \mathbf{d}_i$.

Transforming Eq. (2) into the eigenbasis of Eq. (1) reveals connections between ring eigenstates by optical processes. This is shown in the top panels of Fig. 2 for the case of an $N = 4$ ring (quadmer) for both the ||-SA and the GS-SA configuration, in the latter case only for the 'collective dipole' $\mathbf{D}$ (but a full map is given in the SI[30]). States linked by collectively-enhanced transitions – which overlap significantly with Dicke ladder states (*cf.* Fig. 1b) – are shown in the left-most columns, and we henceforth refer to these as *ladder states*. The colouring indicates the relative strengths of the transition matrix elements [1]. It is important to note that ||-SA ladder states possess the highest energy in their respective excitation manifolds, whereas the opposite is the case for GS-SA.

Reflecting the condensed-matter nature of

---

[1] These are symmetric with respect to absorption and emission (detailed balance follows from asymmetric rates), and they include the cubic frequency dependence of the free space spectral density of optical modes.[34]
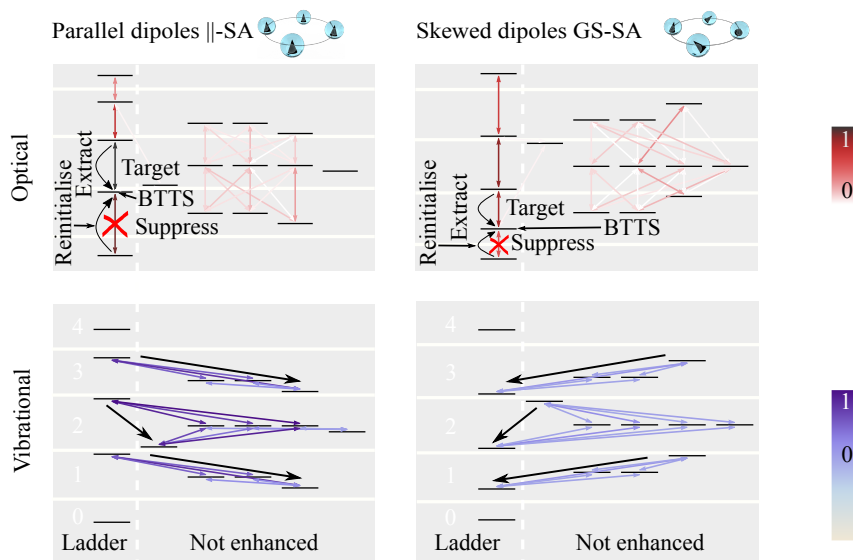
Figure 2: Process diagram showing optical (red, top) and vibrational (blue, bottom) processes linking the eigenstates for a quadmer in the ||-SA (left) and GS-SA (right) setup; normalised colour denotes relative strengths. The states are organised in manifolds corresponding to the number of excitations in the system; the manifolds are visually separated by gaps in the background shading (for clarity energetic intra and inter manifold spacings are not to scale). Optical processes link different manifolds whereas vibrational ones act 'sideways'. Superabsorption is achieved by pairing a reinitialisation process with a suppression of optical decay below the collectively-enhanced 'target' transition. Black arrows show how the GS-SA system is stabilised by vibrational relaxation, whereas for ||-SA phonons are detrimental, pulling the system away from superabsorbing states.

typical nanostructures, we introduce local vibrational baths which are generically coupled to each 2LS via:[37]

$$\hat{H}_{I,\mathrm{vib}} = \sum_{i=1}^{N} \hat{\sigma}_i^z \otimes \sum_q g_{i,q}(\hat{b}_{i,q} + \hat{b}_{i,q}^\dagger) \ , \qquad (3)$$

where $g_{i,q}$ and $\hat{b}_{i,q}^{(\dagger)}$ are, respectively, the coupling strength and annihilation (creation) operator for the phonon mode q for the bath associated with site i.[12,34]

The bottom panels of Fig. 2 show the resulting phonon processes linking quadmer eigenstates for ||-SA and GS-SA, colour-coded to indicate relative strength [2]. Phonon processes only link states within the same excitation manifold and typically occur on a much faster timescale than optical processes. Obeying detailed balance, vibrational relaxation preferentially occurs 'downwards' in energy.[38,39] For ||-SA this implies that phonons exert a pull away

from the ladder linked by enhanced optical processes, ruining the suitability of this configuration for steady-state superabsorption (full details in the SI[30]). By contrast, for GS-SA vibrational dissipation guides the system back to this ladder. A ring of skewed dipoles therefore meets all requirements I-III, and from hereon we shall focus on this configuration.

Wishing to exploit the large oscillator strength at the ladder mid-point, we define a 'target transition' with frequency ω_{good}. As states near the middle of the ladder are not naturally substantially populated, additional measures are required for pinning the system at the 'bottom-of-the-target-transition-state' (BTTS). Let the frequency of the ladder transition immediately below the BTTS be ω_{bad}. Following Ref.,[19] spectral selectivity permits the application of environmental suppression of certain optical modes. Given a sufficient gap between ω_{good} and ω_{bad} (which is proportional to $|J_{i,j}|$), optical decay from the BTTS can be suppressed using a photonic band-gap

---

[2]This is based on an structureless Ohmic phonon spectral density.

environment. Fig. 1c shows that the transition frequencies of upwards absorption (green) and downwards emission (red) processes from the BTTS are indeed well-separated, meaning suppression of a single band of wavelengths will be effective: for GS-SA one may thus suppress all modes with frequency $\omega < (\omega_{\mathrm{good}} + \omega_{\mathrm{bad}})/2$ (see Fig. 1c). A detailed discussion of the suppression of optical processes and separation of desirable and undesirable frequencies, including for ||-SA, is given in the SI.[30]

Suppressing emission from the BTTS prolongs the system's proclivity for remaining in this state, keeping it primed for superabsorbing behaviour. However, an initially excited ring may nonetheless relax towards the ground state at longer times. Addressing this issue requires a physical excitation process which keeps pushing the ring system towards the centre of the ladder. This can be accomplished in two distinct ways: first, the spectrally selective suppression naturally allows the system to passively ratchet itself up to the BTTS, and we found this works well for higher levels of optical suppression. Second, for a lower degree of suppression, an actively controlled excitation process can be added. The latter can be modelled, in an idealised fashion, as incoherent pumping into the BTTS with rate γ_r from all ladder states below the BTTS (or alternatively and more realistically using potentially loss-inducing mechanisms like pumping higher energy states in the manifolds, or even the individual dipoles[30]). In either case, a suitable combination of suppression and (passive or active) reinitialisation achieves significant steady-state population in the BTTS. To be conservative, we shall in the following primarily consider the more involved case of active reinitialisation. Naturally, this incurs a power cost to the operation, so that we will be interested in producing a total power output that is sufficiently high to cover any reinitialisation power cost and still leaves positive net produced power for light-harvesting.

To extract the energy of absorbed photons, we introduce a central trap that is equidistant from all absorbers, analogous to a photosynthetic reaction centre.[20,21] Following the quantum heat engine model,[7,8,40] the trap is modelled as a 2LS

with energy $\omega_t = \omega_{\mathrm{good}}$, whose (incoherent) decay to the ground state at rate γ_t represents the energy conversion process.[3]

Defining the steady-state population of the trap's excited and ground states as $\langle \rho_\alpha \rangle_{SS}$ and $\langle \rho_\beta \rangle_{SS}$, respectively, we assign a hypothetical current and voltage[7,40]

$$I = e\gamma_t \langle \rho_\alpha \rangle_{SS} \;, \quad eV = \omega_t + k_B T_{\mathrm{vib}} \ln\left(\frac{\langle \rho_\alpha \rangle_{SS}}{\langle \rho_\beta \rangle_{SS}}\right),$$
$$(4)$$

where k_B is Boltzmann's constant and $T_{\mathrm{vib}} = 300$ K is the ambient (phonon) temperature. The second term in the voltage expression ensures thermodynamic consistency.[30] Optimising the 'load' via γ_t yields the maximally achievable output power $P_{\mathrm{max}} = I(\gamma_t^*) \cdot V(\gamma_t^*)$ at optimal γ_t^*. To obtain the net power of such a photocell, we must account for the energetic expenditure associated with the reinitialisation process. To this end, we apply a similar concept to the reinitialisation process: we assign a voltage and (upwards current) for each reinitialisation step and sum over the respective products to obtain the total reinitialisation power [4].

We now proceed to solve the dynamics using a Bloch-Redfield approach:[34] non-secular Bloch-Redfield dissipators are formed from the optical, Eq. (2), and vibrational, Eq. (3), Hamiltonians. This approach is most appropriate for relatively weak vibrational coupling, but we discuss the case strongly coupled vibrational baths in the polaron frame[43] in the SI.[30] Apart from the (half-sided) photonic band-gap, we use the free-space optical spectral density, and assume radiative equilibrium with the sun, $T_{\mathrm{opt}} = 5800$ K.[12,44] Phonon processes are based on an Ohmic room-temperature bath, with typical rates exceeding optical ones by three orders of magnitude. Further dissipators describe extraction, trap decay and reinitialisation processes. The chosen extraction rate γ_x is comparable to that of typical phonon processes. The

---

[3] Incoherent decay of a single 2LS can qualitatively capture the effect of exciton transfer down a chain of sites in a tight-binding model.[41,42]

[4] We have here dropped the second term in the voltage definition of Eq. (4). This is a conservative choice and errs on the side of caution: it will over- rather than underestimate the input power.[30]

steady state of the system is then obtained as the nullspace of the total Liouvillian; full details of this process, all parameters, photon and phonon spectral densities, and the explicit master equation can be found in the SI.[30]

Results – First we explore the interplay between the degree of suppression and actively applied reinitialisation. As a function of these parameters, Figs. 3a and b show, respectively, the net power produced and the fraction of expended input vs output power, both for the case of a pentamer. For poor suppression, the system easily leaks down from the BTTS, potentially even resulting in a negative overall power balance (white region) under faster reinitialisation. In an intermediate suppression regime, active reinitialisation becomes worthwhile, so that faster reinitialisation improves performance further. In this regime, the low fraction of output power that is re-invested into active reinitialisation (see Fig. 3b) indicates net power is not at risk of being easily overcome, even when a practical implementation for reinitialisation proves to be somewhat more energetically costly than assumed in our analysis. Finally, for high optical suppression the guide-slide effect successfully produces substantial (net) power in the absence of active reinitialisation, see Fig. 3d for an illustration of this transition into passively self-reinitialising operation. A longer discussion on how suppression enables passive 'free' reinitialisation can be found in Sec. IC of the SI.[30]

To demonstrate superabsorption, i.e. superlinear scaling of photon absorption and energy conversion, we now investigate the effect of increasing the ring-size N. Fig. 4a shows target transition oscillator strength as a function of N: we see that GS-SA displays superlinear scaling for $N > 3$ but trails behind ||-SA and the uncoupled Dicke model [5], due to a combination of employing interacting and skewed dipoles. A similar departure from the quadratic scaling of the idealised Dicke model has also recently been observed experimentally for colour centres in diamond owing to system inhomo-

Figure 3: a) Net power produced by a pentamer as a function of decay suppression and reinitialisation rate. b) Ratio of the power in against the power out across the same parameter scan. c) A cross-section at 99% optical suppression for varying N. d) How different suppression strengths affect net power production without reinitialisation. Dashed lines denote 100% suppression. Full details of the parameters used are in the SI.[30]

---

[5]Note that the gradient changes every two data points since the target transition lies at the centre of the ladder for a ring with an odd N, whereas for an even-sized ring it sits just below the middle
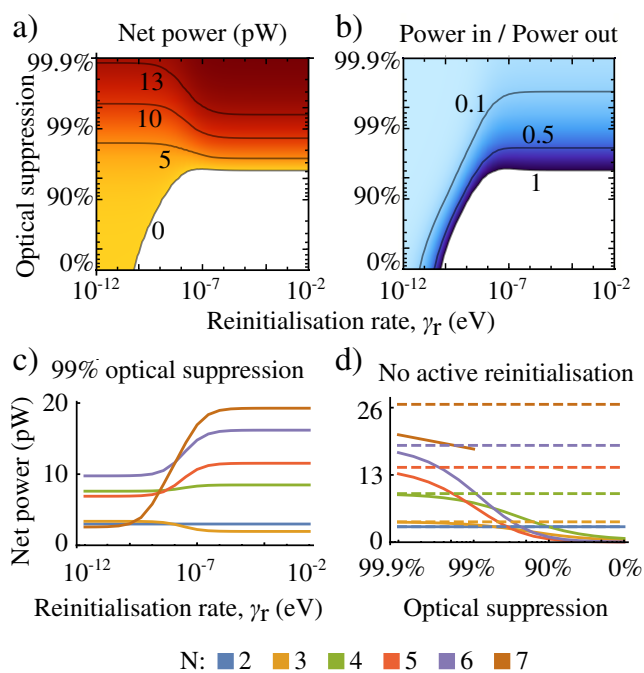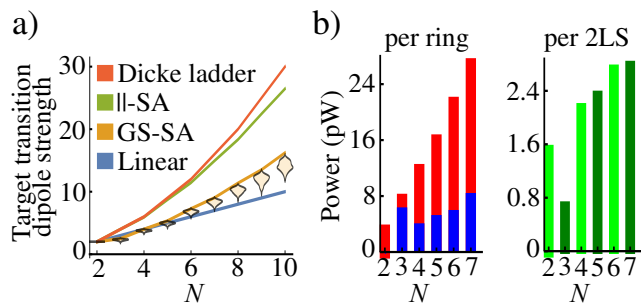
Figure 4: a) Scaling of oscillator strength of the light-havesting target-transition with system size for the different scenarios discussed in the main text. For GS-SA we also include the beige patches corresponding to distributions for 5% disorder introduced across model parameters (10 000 trials for up to $N = 7$, then 1 000, 500 and 50 trials for $N = 8, 9, 10$, respectively). b) Output (red) and input (blue) power for different system sizes with 99% suppression of undesired optical modes, and superlinear growth of net power per site (green). Full details of the parameters used are in the SI.[30]

geneities.[45] Encouragingly, our predicted superlinear GS-SA advantage persists upon introducing 5% normally-distributed disorder amongst relevant parameters (energy splittings ω_A, natural lifetimes τ_L, positions $\mathbf{r}_i$, and dipole orientations), as shown by the pale distribution marks. Further information regarding disorder can be found in the SI.[30]

Focusing on the generated net power, Fig. 3c shows the transition into the guide-slide regime for $2 \le N \le 7$ as a function of γ_r as active reinitialisation is implemented for fixed suppression at 99%. Once γ_r becomes large enough to compensate for (suppressed) optical leakage from the BTTS, larger rings do indeed achieve higher net power. This superlinear growth of the net power with N is confirmed by Fig. 4b, which also gives a breakdown of input vs output power. We note that the dimer and trimer are special: the former performs well as it does not require reinitialisation, whereas the latter has insufficient collective-enhancement for making active reinitialisation worthwhile (but performs adequately left to its own devices, see SI[30]). Beyond $N > 3$, however, there is an increasing trend of GS-SA enabling quantum-
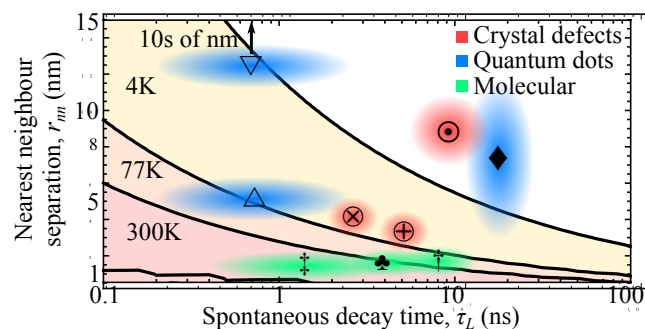
enhanced photocell performance.

Figure 5: Map of where a quadmer produces positive net power as a function of 2LS natural lifetime and nearest neighbour separation. Regions typical of potential candidate systems are overlaid: Adjacent ($\triangledown$) and stacked ($\triangle$) self-assembled InGaS quantum dots.[46,47] $\diamondsuit$: Colloidal quantum dots.[48,49] $\odot$: Nitrogen vacancies.[45,50,51] $\otimes$: Silicon vacancy centres.[52–54] $\oplus$: Phosphorous defects.[55–57] ♣: BODIPY dye.[58–61] †: Porphyrin rings.[25,62,63] ‡: Merocyanine dye (H-aggregate) and pseudoisocyanine chloride (J-aggregate).[64–67]

Focusing on the example of a quadmer we explore the temperature dependence of the effect. As a function of the 2LS spontaneous emission time τ_L and nearest neighbour separation $|\mathbf{r}_{i,i+1}|$ – the key parameters which determine the oscillator and Förster coupling strengths – we map out the region achieving net positive power for different phonon temperatures in Fig. 5. For this purpose, the dipole orientation angles were optimised, but never departed far from our previously employed (slightly suboptimal) ad-hoc choice of $\theta_{\mathrm{eq}} = \pi/2, \theta_{\mathrm{zen}} = \pi/4$ (see Fig. S3[30] for the typical dependence of net power on the dipolar offset angles). Fig. 5 shows that cooling below room temperature expands the working range of GS-SA, since a colder phonon environment boosts the directionality of 'guide-sliding' onto ladder states even for closely spaced levels within the manifold (i.e. weaker Förster couplings).

To address the question of potential candidate systems suitable for exploring the GS-SA effect, we indicate regions and data-points referring to the properties of several state-of-the-art platforms for nanostructure photonics. This

demonstrates a broad range of credible building blocks for GS-SA antennae, leaving the key challenges of (i) ring assembly with control over the direction of the optical dipoles,[6] (ii) embedding into a suitably engineered photonic environment, and (iii) furnishing the antennae with efficient energy extraction[69–71] and reinitialisation channels. Finally, of particular relevance to molecular systems, exciton-exciton annihilation needs to be controlled or avoided.[12] The possibility of constructing molecular light-harvesting ring systems of dyes has already been considered using DNA origami,[72] though the separations are currently larger than desired for room temperature GS-SA applications. A detailed discussion of the effect of non-radiative decay processes in these systems can be found in the SI.[30]

Summary – We have proposed a set of intuitive requirements for guide-slide superabsorption. We have shown that frequency-selective passive reinitialisation via photonic band-gap suppression and, if required, additional active reinitialisation results in a superabsorbing steady-state, characterised by a superlinear scaling of optical absorption and net power conversion with increasing system size. Inspired by photosynthetic structures, we have presented an example ring-system exhibiting this effect. Our proposed setup not only remains viable in the presence of phonons, but even benefits from vibrational relaxation. Further, the effect proves remarkably robust to substantial amounts of disorder and realistic imperfections, showing promise for experimental exploration across a number of platforms. Importantly, bio-inspired molecular rings, similar to the ones described in Refs.,[25,62] could function at room-temperature, offering an exciting perspective for nanophotonics, quantum-enhanced light-harvesting, and possibly future approaches to organic photovoltaics.

---

[6]In crystal defects, possible dipole angles are set by the axis of the crystal,[68] potentially restricting possible configurations which could be synthesised in a single bulk crystal.

Supporting Information Available

Full details of the model used in the main text; more detail on the light-matter and inter-dipole coupling for non-parallel optical dipoles, the construction of the optical and vibrational Bloch-Redfield tensors, and our method for finding steady state solutions; the breakdown of ||-SA and the robustness of GS-SA in the presence of phonons; the effect of non-radiative recombination; optimising the skew dipole orientation for GS superabsorption; a discussion of passive vs active reinitialisation; confirming the integrity of superlinear GS-SA scaling for a range of extensions and variations; disorder applied to the GS-SA model.

References

(1) Blankenship, R. E. *Molecular mechanisms of photosynthesis*, 2nd ed.; John Wiley & Sons, 2014.

(2) Scholes, G. D.; Fleming, G. R.; Olaya-Castro, A.; van Grondelle, R. Lessons from nature about solar light harvesting. *Nat. Chem.* **2011**, *3*, 763.

(3) Romero, E.; Novoderezhkin, V. I.; van Grondelle, R. Quantum design of photosynthesis for bio-inspired solar-energy conversion. *Nature* **2017**, *543*, 355 EP –.

(4) Scholes, G. D.; Fleming, G. R.; Chen, L. X.; Aspuru-Guzik, A.; Buchleitner, A.; Coker, D. F.; Engel, G. S.; van Grondelle, R.; Ishizaki, A.; Jonas, D. M. et al. Using coherence to enhance function in chemical and biophysical systems. *Nature* **2017**, *543*, 647 EP –.

(5) Shockley, W.; Queisser, H. J. Detailed Balance Limit of Efficiency of pâĂŘn Junction Solar Cells Theoretical efficiency limit for a two-terminal multi-junction " step-cell " using detailed balance method Detailed Balance Limit of Efficiency of p-n Junction Solar Cells*. *J. Appl. Phys.* **1961**, *32*.

(6) Scully, M. O. Quantum Photocell: Using Quantum Coherence to Reduce Radiative Recombination and Increase Efficiency. *Phys. Rev. Lett.* **2010**, *104*, 207701.

(7) Scully, M. O.; Chapin, K. R.; Dorfman, K. E.; Kim, M. B.; Svidzinsky, A. Quantum heat engine power can be increased by noise-induced coherence. *Proc. Natl. Acad. Sci. U.S.A.* **2011**, *108*, 15097–100.

(8) Creatore, C.; Parker, M. A.; Emmott, S.; Chin, A. W. Efficient Biologically Inspired Photocell Enhanced by Delocalized Quantum States. *Phys. Rev. Lett.* **2013**, *111*, 253601.

(9) Yamada, Y.; Yamaji, Y.; Imada, M. Exciton Lifetime Paradoxically Enhanced by Dissipation and Decoherence: Toward Efficient Energy Conversion of a Solar Cell. *Phys. Rev. Lett.* **2015**, *115*, 197701.

(10) Fruchtman, A.; Gómez-Bombarelli, R.; Lovett, B. W.; Gauger, E. M. Photocell Optimization Using Dark State Protection. *Phys. Rev. Lett.* **2016**, *117*, 203603.

(11) Zhang, Y.; Oh, S.; Alharbi, F. H.; Engel, G. S.; Kais, S. Delocalized quantum states enhance photocell efficiency. *Phys. Chem. Chem. Phys.* **2015**, *17*, 5743–5750.

(12) Higgins, K. D. B.; Lovett, B. W.; Gauger, E. M. Quantum-Enhanced Capture of Photons Using Optical Ratchet States. *J. Phys. Chem. C* **2017**, *121*, 20714–20719.

(13) Zhang, Y.; Wirthwein, A.; Alharbi, F. H.; Engel, G. S.; Kais, S. Dark states enhance

the photocell power via phononic dissipation. *Phys. Chem. Chem. Phys.* **2016**, *18*, 31845–31849.

(14) Hu, Z.; Engel, G. S.; Kais, S. Double-excitation manifold's effect on exciton transfer dynamics and the efficiency of coherent light harvesting. *Phys. Chem. Chem. Phys.* **2018**, *20*, 30032–30040.

(15) Killoran, N.; Huelga, S. F.; Plenio, M. B. Enhancing light-harvesting power with coherent vibrational interactions: A quantum heat engine picture. *J. Chem. Phys.* **2015**, *143*.

(16) Stones, R.; Hossein-Nejad, H.; van Grondelle, R.; Olaya-Castro, A. On the performance of a photosystem II reaction centre-based photocell. *Chem. Sci.* **2017**, *8*, 6871–6880.

(17) Tomasi, S.; Baghbanzadeh, S.; Rahimi-Keshari, S.; Kassal, I. Coherent and controllable enhancement of light-harvesting efficiency. **2018**,

(18) Dicke, R. H. Coherence in Spontaneous Radiation Processes. *Phys. Rev.* **1954**, *93*, 99–110.

(19) Higgins, K. D. B.; Benjamin, S. C.; Stace, T. M.; Milburn, G. J.; Lovett, B. W.; Gauger, E. M. Superabsorption of light via quantum engineering. *Nat. Commun.* **2014**, *5*, 4705.

(20) Law, C. J.; Roszak, A. W.; Southall, J.; Gardiner, A. T.; Isaacs, N. W.; Cogdell, R. J. The structure and function of bacterial light-harvesting complexes (Review). *Mol. Membr. Biol.* **2004**, *21*, 183–191.

(21) Sumi, H. Bacterial photosynthesis begins with quantum-mechanical coherence. *The Chemical Record* **2001**, *1*, 480–93.

(22) Hu, X.; Ritz, T.; Damjanović, A.; Schulten, K. Pigment Organization and Transfer of Electronic Excitation in the Photo-

synthetic Unit of Purple Bacteria. *J. Phys. Chem. B* **1997**, *101*, 3854–3871.

(23) Takahashi, S.; Badger, M. R. Photoprotection in plants: a new light on photosystem II damage. *Trends Plant Sci.* **2011**, *16*, 53–60.

(24) Yang, D.; Oh, S.-h.; Han, J.; Son, G.; Kim, J.; Kim, J.; An, K. Observation of superabsorption by correlated atoms. *arXiv preprint arXiv:1906.06477* **2019**,

(25) O'Sullivan, M. C.; Sprafke, J. K.; Kondratuk, D. V.; Rinfray, C.; Claridge, T. D. W.; Saywell, A.; Blunt, M. O.; O'Shea, J. N.; Beton, P. H.; Malfois, M. et al. Vernier templating and synthesis of a 12-porphyrin nano-ring. *Nature* **2011**, *469*, 72–75.

(26) Butkus, V.; Alster, J.; Bašinskaitė, E.; Augulis, R.; Neuhaus, P.; Valkunas, L.; Anderson, H. L.; Abramavicius, D.; Zigmantas, D. Discrimination of Diverse Coherences Allows Identification of Electronic Transitions of a Molecular Nanoring. *J. Phys. Chem. Lett.* **2017**, *8*, 2344–2349.

(27) Prasanna Venkatesh, B.; Juan, M. L.; Romero-Isart, O. Cooperative Effects in Closely Packed Quantum Emitters with Collective Dephasing. *Phys. Rev. Lett.* **2018**, *120*, 033602.

(28) Gullì, M.; Valzelli, A.; Mattiotti, F.; Angeli, M.; Borgonovi, F.; Celardo, G. L. Macroscopic coherence as an emergent property in molecular nanotubes. *New J. Phys.* **2019**, *21*, 013019.

(29) Löhner, A.; Kunsel, T.; Röhr, M. I. S.; Jansen, T. L. C.; Sengupta, S.; Würthner, F.; Knoester, J.; Köhler, J. Spectral and Structural Variations of Biomimetic Light-Harvesting Nanotubes. *J. Phys. Chem. Lett.* **2019**, 2715–2724.

(30) See Supplemental Material at [URL will be inserted by publisher] for further de-
tail, model extensions and disorder calculations.

(31) Gross, M.; Haroche, S. Superradiance: An essay on the theory of collective spontaneous emission. *Phys. Rep.* **1982**, *93*, 301–396.

(32) Varada, G. V.; Agarwal, G. S. Two-photon resonance induced by the dipole-dipole interaction. *Phys. Rev. A* **1992**, *45*, 6721–6729.

(33) Curutchet, C.; Mennucci, B. Quantum Chemical Studies of Light Harvesting. *Chem. Rev.* **2017**, *117*, 294–343.

(34) Breuer, H.-P.; Petruccione, F. *The Theory of Open Quantum Systems*; Oxford University Press, 2002.

(35) Agarwal, G. S. *Quantum statistical theories of spontaneous emission and their relation to other approaches*; Springer, Berlin, Heidelberg, 1974; pp 1–128.

(36) Shatokhin, V. N.; Walschaers, M.; Schlawin, F.; Buchleitner, A. Coherence turned on by incoherent light. *New J. Phys.* **2018**, *20*, 113040.

(37) Mahan, G. D. *Many Particle Physics (Physics of Solids and Liquids)*, 3rd ed.; Springer, 2000.

(38) Gauger, E. M.; Wabnig, J. Heat pumping with optically driven excitons. *Phys. Rev. B* **2010**, *82*, 073301.

(39) Ramsay, A. J.; Godden, T. M.; Boyle, S. J.; Gauger, E. M.; Nazir, A.; Lovett, B. W.; Gopal, A. V.; Fox, A. M.; Skolnick, M. S. Effect of detuning on the phonon induced dephasing of optically driven InGaAs/GaAs quantum dots. *J. Appl. Phys.* **2011**, *109*, 102415.

(40) Dorfman, K. E.; Voronine, D. V.; Mukamel, S.; Scully, M. O. Photosynthetic reaction center as a quantum heat engine. *Proc. Natl. Acad. Sci. U.S.A.* **2013**, *110*, 2746–51.

(41) Giusteri, G. G.; Mattiotti, F.; Celardo, G. L. Non-Hermitian Hamiltonian approach to quantum transport in disordered networks with sinks: Validity and effectiveness. *Phys. Rev. B* **2015**, *91*, 094301.

(42) Schaller, G.; Giusteri, G. G.; Celardo, G. L. Collective couplings: Rectification and supertransmittance. *Phys. Rev. E* **2016**, *94*, 032135.

(43) Nazir, A.; McCutcheon, D. P. S. Modelling exciton–phonon interactions in optically driven quantum dots. *J. Phys. Condens. Matter* **2016**, *28*, 103002.

(44) Würfel, P.; Würfel, U. *Physics of Solar Cells: From Basic Principles to Advanced Concepts*, 3rd ed.; Wiley-VCH, 2016.

(45) Angerer, A.; Streltsov, K.; Astner, T.; Putz, S.; Sumiya, H.; Onoda, S.; Isoya, J.; Munro, W. J.; Nemoto, K.; Schmiedmayer, J. et al. Superradiant emission from colour centres in diamond. *Nat. Phys.* **2018**, *14*, 1168–1172.

(46) Creasey, M.; Lee, J.-H.; Wang, Z.; Salamo, G. J.; Li, X. Self-Assembled InGaAs Quantum Dot Clusters with Controlled Spatial and Spectral Properties. *Nano Lett.* **2012**, *12*, 5169–5174.

(47) Gerardot, B. D.; Strauf, S.; de Dood, M. J. A.; Bychkov, A. M.; Badolato, A.; Hennessy, K.; Hu, E. L.; Bouwmeester, D.; Petroff, P. M. Photon Statistics from Coupled Quantum Dots. *Phys. Rev. Lett.* **2005**, *95*, 137403.

(48) Lounis, B.; Bechtel, H.; Gerion, D.; Alivisatos, P.; Moerner, W. Photon antibunching in single CdSe/ZnS quantum dot fluorescence. *Chem. Phys. Lett.* **2000**, *329*, 399–404.

(49) Brichkin, S. B.; Razumov, V. F. Colloidal quantum dots: synthesis, properties and applications. *Russ. Chem. Rev.* **2016**, *85*, 1297–1312.

(50) Albrecht, A.; Koplovitz, G.; Retzker, A.; Jelezko, F.; Yochelis, S.; Porath, D.; Nevo, Y.; Shoseyov, O.; Paltiel, Y.; B Plenio, M. Self-assembling hybrid diamond–biological quantum devices. *New J. Phys.* **2014**, *16*, 093002.

(51) Neumann, P.; Kolesov, R.; Naydenov, B.; Beck, J.; Rempp, F.; Steiner, M.; Jacques, V.; Balasubramanian, G.; Markham, M. L.; Twitchen, D. J. et al. Quantum register based on coupled electron spins in a room-temperature solid. *Nat. Phys.* **2010**, *6*, 249–253.

(52) Rogers, L.; Jahnke, K.; Teraji, T.; Marseglia, L.; Müller, C.; Naydenov, B.; Schauffert, H.; Kranz, C.; Isoya, J.; McGuinness, L. et al. Multiple intrinsically identical single-photon emitters in the solid state. *Nat. Commun.* **2014**, *5*, 4739.

(53) Sipahigil, A.; Evans, R. E.; Sukachev, D. D.; Burek, M. J.; Borregaard, J.; Bhaskar, M. K.; Nguyen, C. T.; Pacheco, J. L.; Atikian, H. A.; Meuwly, C. et al. An integrated diamond nanophotonics platform for quantum-optical networks. *Science* **2016**, *354*, 847–850.

(54) Morse, K. J.; Abraham, R. J. S.; DeAbreu, A.; Bowness, C.; Richards, T. S.; Riemann, H.; Abrosimov, N. V.; Becker, P.; Pohl, H.-J.; Thewalt, M. L. W. et al. A photonic platform for donor spin qubits in silicon. *Sci. Adv.* **2017**, *3*, e1700930.

(55) O'Brien, J. L.; Schofield, S. R.; Simmons, M. Y.; Clark, R. G.; Dzurak, A. S.; Curson, N. J.; Kane, B. E.; McAlpine, N. S.; Hawley, M. E.; Brown, G. W. Towards the fabrication of phosphorus qubits for a silicon quantum computer. *Phys. Rev. B* **2001**, *64*, 161401.

(56) Fuechsle, M.; Miwa, J. A.; Mahapatra, S.; Ryu, H.; Lee, S.; Warschkow, O.; Hollenberg, L. C. L.; Klimeck, G.; Sim-

mons, M. Y. A single-atom transistor. *Nat. Nanotechnol.* **2012**, *7*, 242–246.

(57) Schofield, S. R.; Curson, N. J.; Simmons, M. Y.; Rueß, F. J.; Hallam, T.; Oberbeck, L.; Clark, R. G. Atomically Precise Placement of Single Dopants in Si. *Phys. Rev. Lett.* **2003**, *91*, 136104.

(58) Berezin, M. Y.; Achilefu, S. Fluorescence lifetime measurements and biological imaging. *Chem. Rev.* **2010**, *110*, 2641–84.

(59) Pochorovski, I.; Knehans, T.; Nettels, D.; Müller, A. M.; Schweizer, W. B.; Caflisch, A.; Schuler, B.; Diederich, F. Experimental and Computational Study of BODIPY Dye-Labeled Cavitand Dynamics. *J. Am. Chem. Soc.* **2014**, *136*, 2441–2449.

(60) Acikgoz, S.; Aktas, G.; Inci, M. N.; Altin, H.; Sanyal, A. FRET between BODIPY Azide Dye Clusters within PEG-Based Hydrogel: A Handle to Measure Stimuli Responsiveness. *J. Phys. Chem. B* **2010**, *114*, 10954–10960.

(61) Chung, P.-H.; Tregidgo, C.; Suhling, K. Determining a fluorophore's transition dipole moment from fluorescence lifetime measurements in solvents of varying refractive index. *Methods Appl. Fluoresc.* **2016**, *4*, 045001.

(62) Sprafke, J. K.; Kondratuk, D. V.; Wykes, M.; Thompson, A. L.; Hoffmann, M.; Drevinskas, R.; Chen, W.-H.; Yong, C. K.; Kärnbratt, J.; Bullock, J. E. et al. Belt-Shaped π-Systems: Relating Geometry to Electronic Structure in a Six-Porphyrin Nanoring. *J. Am. Chem. Soc.* **2011**, *133*, 17262–17273.

(63) Yu, J.; Wang, X.; Zhang, B.; Weng, Y.; Zhang, L. Prolonged Excited-State Lifetime of Porphyrin Due to the Addition of Colloidal SiO2 to Triton X-100 Micelles. *Langmuir* **2004**,

(64) Rösch, U.; Yao, S.; Wortmann, R.; Würthner, F. Fluorescent H-Aggregates of Merocyanine Dyes. *Angew. Chem.* **2006**, *45*, 7026–7030.

(65) Würthner, F. Dipole–Dipole Interaction Driven Self-Assembly of Merocyanine Dyes: From Dimers to Nanoscale Objects and Supramolecular Materials. *Acc. Chem. Res.* **2016**, *49*, 868–876.

(66) Obara, Y.; Saitoh, K.; Oda, M.; Tani, T. Room-temperature fluorescence lifetime of pseudoisocyanine (PIC) J excitons with various aggregate morphologies in relation to microcavity polariton formation. *Int. J. Mol. Sci.* **2012**, *13*, 5851–65.

(67) von Berlepsch, H.; Böttcher, C.; Dähne, L. Structure of J-Aggregates of Pseudoisocyanine Dye in Aqueous Solution. *J. Phys. Chem. B* **2000**, *104*, 8792–8799.

(68) Doherty, M. W.; Manson, N. B.; Delaney, P.; Jelezko, F.; Wrachtrup, J.; Hollenberg, L. C. The nitrogen-vacancy colour centre in diamond. *Phys. Rep.* **2013**, *528*, 1–45.

(69) Dubi, Y. Interplay between Dephasing and Geometry and Directed Heat Flow in Exciton Transfer Complexes. *J. Phys. Chem. C* **2015**, *119*, 25252–25259.

(70) Baghbanzadeh, S.; Kassal, I. Geometry, Supertransfer, and Optimality in the Light Harvesting of Purple Bacteria. *J. Phys. Chem. Lett.* **2016**, *7*, 3804–3811.

(71) Zhang, Y.; Celardo, G. L.; Borgonovi, F.; Kaplan, L. Opening-assisted coherent transport in the semiclassical regime. *Phys. Rev. E* **2017**, *95*, 022122.

(72) Hemmig, E. A.; Creatore, C.; Wünsch, B.; Hecker, L.; Mair, P.; Parker, M. A.; Emmott, S.; Tinnefeld, P.; Keyser, U. F.; Chin, A. W. Programming Light-Harvesting Efficiency Using DNA Origami. *Nano Lett.* **2016**, *16*, 2369–2374.